COMMUNICATION

Check for updates

Ultrathin and permeable silver nanowires/polyvinyl alcohol epidermal electrode for continuous electrophysiological monitoring†

Junhong Yi, [ID] [a] Yuheng Gu, [ID] [a] Jiawei Yang, [ab] Zonglei Wang, [ab] Yuli Wang, [ab] Wenqing Yan, [a] Qingyuan Sun, [ab] Pengcheng Zhou, [ab] Yumiao Xu, [cd] Xuezhong He, [ab] Junwen Zhong [ID] [e] and Yan Wang [ID] *[abfg]

The development of ultrathin and highly permeable epidermal electrodes is critical for continuous health monitoring, enabling early diagnosis and effective disease management. However, conventional epidermal electrode materials and designs face significant challenges in achieving the necessary combination of ultrathin geometry, gas permeability, seamless adhesion, and high stretchability for long-term wearability. To address these issues, we report an ultrathin gel electrode consisting of a polyvinyl alcohol gel and silver nanowires with a thickness of only 14.7 μm. The high electrical conductivity and nanomaterial reinforcement of silver nanowires, and the flexibility, biocompatibility, and adhesion of polyvinyl alcohol provide silver nanowires/polyvinyl alcohol with excellent performance. This composite structure synergistically combines the strengths of each component, overcoming the limitations of traditional single-material designs, resulting in excellent mechanical properties, including stretchability up to 662% strain, a tensile strength of 1.5 MPa, and a water mist-induced adhesion energy of 270.5 μJ cm^{-2}. Additionally, the gas permeability of the gel electrode is 113 times higher than that of a 100 μm-thick polydimethylsiloxane film, with an air permeance value of 0.03 cm$_{STP}^{3}$ cm^{-2} s^{-1} cmHg^{-1}, resulting in enhanced humidity regulation and improved thermal comfort. In practical applications, the ultrathin silver nanowires/polyvinyl alcohol gel electrode demonstrates outstanding electrophysiological signal acquisition capabilities. Its signal-to-noise ratios for electromyography and electrocardiography match those of commercial gel electrodes, enabling continuous, high-fidelity wireless health monitoring for up to 3 h during daily activities. Furthermore, in electroencephalography measurements, the sensor reliably captures stable alpha waves with minimal background noise, underscoring its excellent real-time frequency response performance.

New concepts

Long-term electrophysiological monitoring systems face limitations due to conventional skin electrodes, which are often bulky, inflexible, and lack sufficient breathability, making them unsuitable for extended wear. To address these challenges, we present an ultrathin silver nanowires/polyvinyl alcohol (AgNWs/PVA) gel with a thickness of just 14.7 μm. The AgNWs create a robust, percolated conductive network within the biocompatible, hydrophilic PVA matrix, significantly improving both electrical conductivity and mechanical strength. Additionally, the intrinsic properties of PVA, such as excellent skin adhesion and moisture retention, ensure the electrode remains securely attached to the skin while promoting comfort during long-term wear. The AgNWs/PVA gel also demonstrates exceptional mechanical properties, including stretchability up to 662% strain, tensile strength of 1.5 MPa, and adhesion energy of 270.5 μJ cm^{-2}, alongside superior air permeance (0.03 cm$_{STP}^{3}$ cm^{-2} s^{-1} cmHg^{-1}), ensuring breathability and thermal comfort. Moreover, the AgNWs/PVA electrode maintains stable, low skin contact impedance signal acquisition, crucial for reliable electrophysiological monitoring, with signal-to-noise ratios comparable to commercial electrodes, enabling continuous and high-fidelity electrophysiological signal acquisition in daily environments.

[a] Department of Chemical Engineering, Guangdong Technion-Israel Institute of Technology, 241 Daxue Road, Shantou, Guangdong 515063, China

[b] The Wolfson Department of Chemical Engineering, Technion-Israel Institute of Technology, Haifa 3200003, Israel. E-mail: wang.yan@technion.ac.il

[c] Department of Materials Science and Engineering, Guangdong Technion-Israel Institute of Technology, 241 Daxue Road, Shantou, Guangdong 515063, China

[d] Department of Materials Science and Engineering, Technion-Israel Institute of Technology, Haifa 3200003, Israel

[e] Department of Electromechanical Engineering and Centre for Artificial Intelligence and Robotics, University of Macau, Macau SAR 999078, China

[f] Guangdong Provincial Key Laboratory of Materials and Technologies for Energy Conversion, Guangdong Technion-Israel Institute of Technology, 241 Daxue Road, Shantou, Guangdong 515063, China

[g] Guangdong Provincial Key Laboratory of Science and Engineering for Health and Medicine, Guangdong Technion-Israel Institute of Technology, Shantou, Guangdong 515063, China

† Electronic supplementary information (ESI) available. See DOI: https://doi.org/10.1039/d4mh01858c

1. Introduction

Electrophysiological monitoring plays a critical role in the early detection and diagnosis of cardiovascular, muscular, and neurological diseases, enabling timely intervention and personalized health management.[1] Devices for monitoring electrophysiological signals, such as electrocardiogram (ECG), electromyogram (EMG), electroencephalogram (EEG), and electrooculogram (EOG), rely heavily on epidermal electrodes.[2] These electrodes have gained widespread adoption due to their biocompatibility, mechanical flexibility, conformability to the skin, and ability to deliver high-precision signal acquisition.[3]

To date, various materials have been explored to fabricate epidermal electrodes, including carbon nanotubes (CNTs),[4] graphene,[5] metal nanowires,[6] liquid metals,[7] and hydrogels.[8] Among these, wet electrodes have garnered significant attention for their low skin-electrode impedance and strong adhesion to the human skin, which result in superior signal quality.[9] For instance, Wang et al. developed a poly(acrylamide-2-acrylamide-2-methylpropane sulfonic acid) hydrogel-based electrode with exceptionally low contact impedance (lower than 300 kΩ at 10 Hz) and high adhesion (158.8 N m^{-1}), enabling its use in EMG monitoring with a signal-to-noise ratio (SNR) of 20.37 dB.[10] Another example is the work of Pan et al., who introduced an alginate-polyacrylamide hydrogel-based electrode with enhanced adhesion (90 N m^{-1}) and mechanical flexibility (over 1800% strain). The developed electrode demonstrated stable and clear signal acquisition during prolonged EMG monitoring, achieving an SNR greater than 23 dB.[11] These studies underscore the potential of wet electrodes in enhancing electrophysiological signal acquisition by improving skin-electrode interface properties.

Despite their advantages in short-term applications, wet electrodes face considerable challenges in long-term continuous health monitoring. Wet electrodes must not only maintain high electrical fidelity but also address issues related to mechanical robustness, adhesion, and most critically, gas permeability in order to achieve sustained performance. Gas permeability plays a pivotal role in ensuring skin comfort and health by facilitating moisture management and preventing the accumulation of sweat and metabolic byproducts, which could otherwise lead to irritation, allergic reactions, or signal degradation. Recent advancements in ultrathin gel epidermal electrodes have demonstrated promising solutions by enhancing permeability while maintaining stretchability and strong adhesion (Table S1, ESI†).[12–21] For example, Li et al. achieved significant improvements in thickness (2–8 μm), permeability (water vapor transmission rate (WVTR) of 18.4 mg cm^{-2} h^{-1}), adhesion (1.32 N cm^{-1}), stretchability (60% strain), and conductivity (sheet resistance of 5.2 Ω sq^{-1}), enabling stable ECG intermittent monitoring for 12 h.[14] Similarly, Zhou et al. reported an ultrathin gel electrode (4.6 μm) optimized for extended wear, showcasing outstanding gas permeability (WVTR of 23 mg cm^{-2} h^{-1}) and robust mechanical properties (tensile stress over 0.9 MPa and stretchability of 350% strain) with applications in ECG monitoring (SNR of 7 dB) and EMG monitoring (SNR of 24.9 dB).[17]

However, the development of gel electrodes that effectively integrate ultrathin geometry, gas permeability, seamless adhesion, and high stretchability remains a significant engineering challenge. Achieving ultrathin geometry is essential for ensuring comfort and minimizing the physical presence of the electrode on the skin.[22] Nevertheless, reducing thickness often leads to compromised mechanical robustness, making the electrode prone to tearing or deformation under strain.[23] Similarly, increasing gas permeability facilitates prolonged wear but may weaken the structural integrity of the electrode. On the other hand, ensuring seamless adhesion is crucial for maintaining stable electrical contact during dynamic movements. However, it often conflicts with the necessary stretchability required to accommodate skin deformation without inducing signal degradation.[24] These interdependent factors create complex design trade-offs, where enhancing one property may inadvertently compromise another. Therefore, innovative material compositions and fabrication strategies are essential to achieving a delicate balance among these competing characteristics, ultimately enabling epidermal electrodes to meet the demands of reliable, continuous, and long-term electrophysiological monitoring. In this regard, polyvinyl alcohol (PVA) has emerged as a promising material for soft electronics due to its biocompatibility, hydrophilicity, cost-effectiveness, and non-toxicity.[25] Moreover, robust PVA gels can be readily fabricated using techniques such as salting-out, solvent exchange, and photo-crosslinking.[26–29] Nevertheless, recent studies have found that while PVA-based gels offer excellent processability and skin compatibility, their inherent mechanical strength and limited electrical conductivity limit their practical applications. This has driven the combination of PVA with conductive nanomaterials to enhance the conductivity and mechanical properties of PVA-based gels.

In this study, we developed a 14.7-μm-thick, stretchable, adhesive, and breathable silver nanowires (AgNWs)/PVA gel electrode. By incorporating AgNWs as a reinforcement, we enhanced both the mechanical strength and electrical conductivity of the gel. The electrode exhibits excellent mechanical properties, including stretchability of 662% strain, 1.5 MPa tensile strength, and strong adhesion (270.5 μJ cm^{-2}), along with great air permeance (0.03 cm$_{STP}^3$ cm^{-2} s^{-1} cmHg^{-1}) and thermal comfort. These features enable the gel to maintain stable performance for long-term electrophysiological monitoring wirelessly under daily wear. These findings highlight the potential of the ultrathin AgNWs/PVA gel as a versatile and reliable solution for next-generation wearable health monitoring systems for personalized healthcare.

2. Result and discussion

2.1. Design and characterization of the ultrathin AgNWs/PVA gel

To effectively balance the mechanical strength of ultrathin materials, reinforcement with nanomaterials has been proven to be a feasible strategy for the fabrication of robust ultrathin

materials.[30] AgNWs, with their nanoscale grain structure and metallic characteristics, provide advantageous mechanical flexibility and high electrical conductivity, leading to widespread applications in electronic skins.[17,27] Therefore, AgNWs were selected as nano-reinforcing agents in the gel matrix to enhance both mechanical strength and electrical conductivity (Fig. 1A).

PVA was chosen as the main matrix due to its excellent hydration and hydrophilicity, which facilitate stable and seamless contact with human skin. Additionally, PVA gels exhibit high flexibility and plasticity in the hydrated state, enabling better adhesion through deformation or self-adaptation.[31,32] Phosphoric acid forms a hydrogen-bonding network with PVA, enhancing adhesion as well as the mechanical strength and water resistance of the material. Its ionized phosphate species further improve electrostatic adhesion to the skin, ensuring robust bonding.[33] Additionally, phosphoric acid promotes better dispersion of AgNWs in the substrate solution, leading to improved electrical conductivity (Fig. S1, ESI†). The preparation process of the AgNWs/PVA gel is detailed in Fig. S2 (ESI†). The ultrathin material conforms to the skin texture and has low gas diffusion resistance for improved adhesion and breathability.[34]

To further achieve an ultrathin structure, the influence of precursor volume and AgNWs concentration on the sample thickness was investigated (Fig. S3 and S4, ESI†). Considering the influence of thickness on the overall performance of AgNWs/PVA gel, such as gas permeability, and adhesion (Fig. S5 and S6, ESI†). In this work, a thickness of 14.7 μm and 1.5 g L^{-1} AgNWs is chosen for skin applicability, referred to hereafter as ultrathin AgNWs/PVA gel unless otherwise stated.

Scanning electron microscopy (SEM) cross-sectional images illustrate that the ultrathin AgNWs/PVA gel has a thickness of only 14.7 μm. (Fig. 1B). And the surface energy dispersive spectroscopy (EDS) result shows that AgNWs are uniformly distributed in the PVA matrix (Fig. 1C). Ultrathin AgNWs/PVA gel adhered seamlessly to the human wrist due to its thin thickness, and its high transparency allows better visualization of the human skin (Fig. S7, ESI†). The surface texture of the attached AgNWs/PVA gel on the human skin was similar to that of the uncovered skin, indicating its capability to adapt to skin texture (Fig. 1D).[35] Furthermore, it is also capable of adhering to human skin for over 16 h under daily activities (Fig. S8, ESI†).
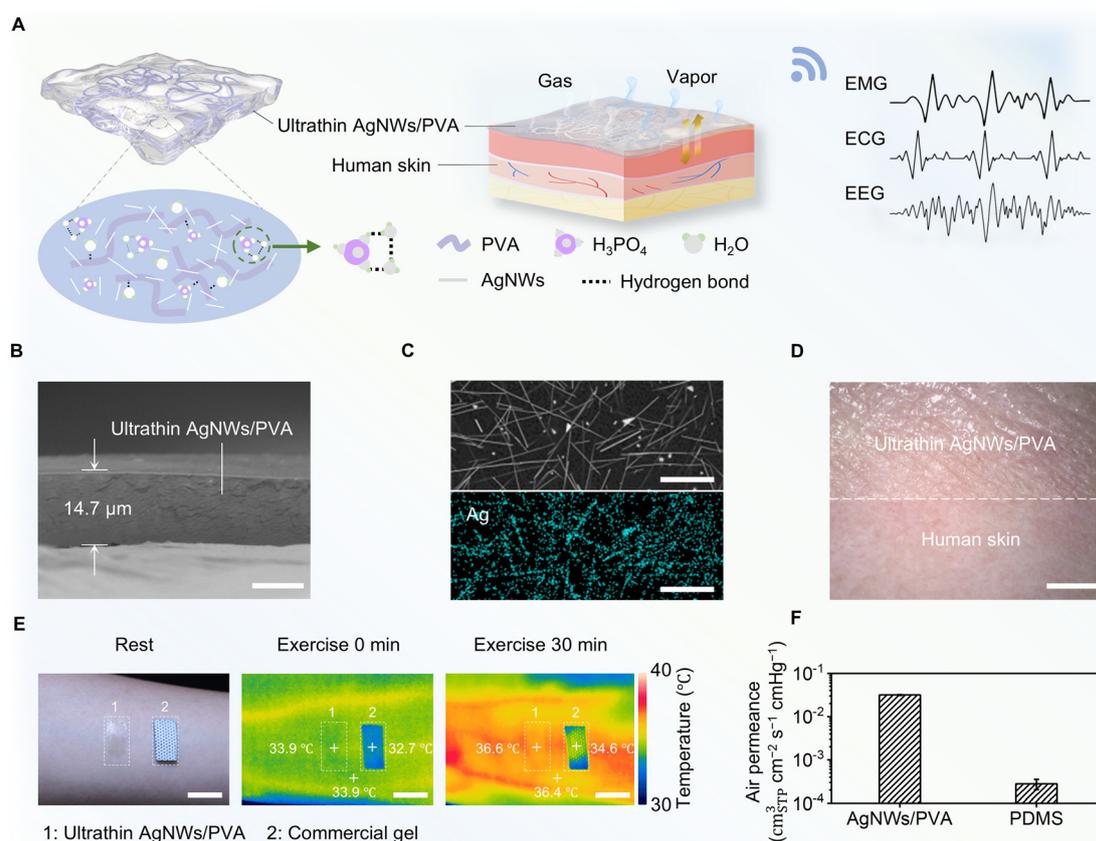
Fig. 1 Ultrathin, gas permeable AgNWs/PVA epidermal electrode. (A) Schematic illustration of ultrathin AgNWs/PVA gel adhered to the human skin for wireless electrophysiological monitoring. (B) Cross-sectional SEM image of ultrathin AgNWs/PVA gel. Scale bar, 10 μm. (C) SEM image (top) and silver element distribution map (bottom) of AgNWs/PVA gel. Scale bar, 10 μm. (D) Microscope image of ultrathin AgNWs/PVA gel attached to human skin. Scale bar, 2 mm. (E) Images of the samples at rest and infrared images of 0 min of exercise and 30 min of exercise. Scale bar, 2 cm. (F) Air permeance of ultrathin AgNWs/PVA gel and 100-μm-thick PDMS film.

To estimate the thermal conductivity, the ultrathin AgNWs/PVA gel and the commercial gel were adhered to the arm separately (Fig. 1E). Infrared imaging indicated that the ultrathin AgNWs/PVA gel had a temperature comparable to the human arm surface, whereas the commercial gel exhibited a significant temperature difference (1.2 °C). After 30 min of exercise, the temperature around the arm increased by 2.5 °C, and the temperature of the ultrathin AgNWs/PVA gel increased by 2.7 °C, whereas the temperature of the commercial gel increased by only 1.9 °C. This result shows that the ultrathin AgNWs/PVA gel has excellent thermal conductivity, enhancing thermal comfort during wear. Furthermore, the contact angle of the ultrathin AgNWs/PVA gel was less than 90°, promoting moisture retention on the skin and reducing dryness and irritation, further supporting its comfort during use (Fig. S9, ESI†). The ultrathin AgNWs/PVA gel significantly enhances skin compliance by reducing flexural rigidity and enabling rapid gas and vapor diffusion from the underlying skin.[12] In addition, the adhesion and electrical performance of the ultrathin AgNWs/PVA gel increase significantly under mild sweating conditions, while the mechanical strength and stretchability decrease. (Fig. S10, ESI†). The air permeance of the ultrathin AgNWs/PVA gel is up to 0.03 cm_{STP}^3 cm^{-2} s^{-1} $cmHg^{-1}$, which is 113 times higher than that of a 100-μm-thick PDMS film (Fig. 1F).

2.2. Mechanical, adhesive, and mechano-electrical characteristics of the AgNWs/PVA gel

To evaluate the practical skin applicability of AgNWs/PVA gel electrode, the mechanical, adhesive, and electrical properties of AgNWs/PVA gel are investigated. Fig. 2A displays the effect of AgNWs concentration (0.5–2.0 g L^{-1}) on the mechanical properties of the gel. As the AgNWs concentration increased, the distribution of AgNWs in the PVA matrix became more homogeneous (Fig. S11, ESI†). At an optimal concentration of 1.5 g L^{-1}, AgNWs/PVA gel achieved a tensile strength of 1.5 MPa and a stretchability of 662% strain, attributable to the uniform
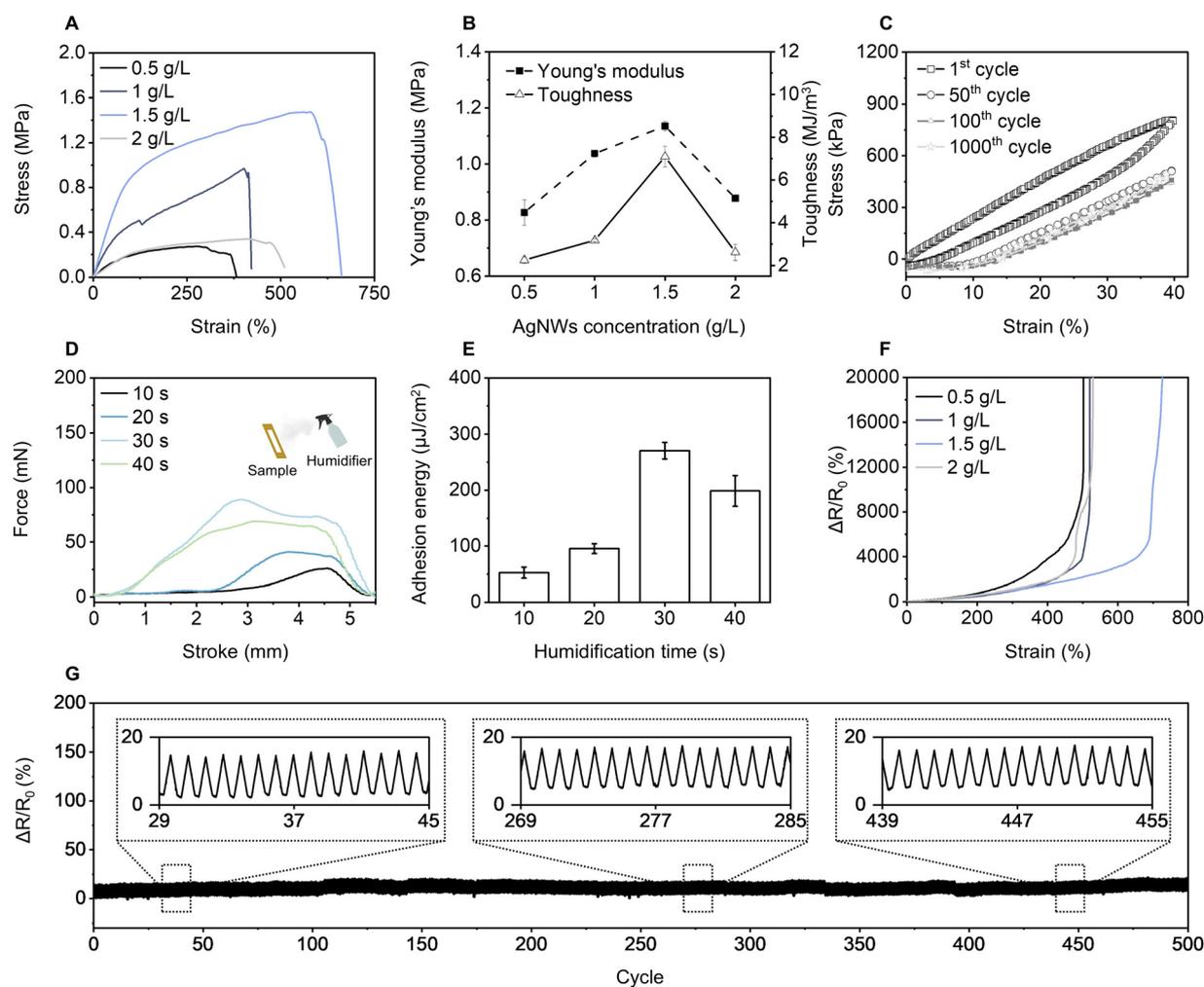

Fig. 2 Mechanical, adhesive, and mechano-electrical characteristics of the AgNWs/PVA gel. (A) Tensile stress curves of AgNWs/PVA gel at different AgNWs concentrations. (B) Young's modulus and toughness of AgNWs/PVA gel across varying AgNWs concentrations. (C) Cyclic stretching/releasing curves of AgNWs/PVA gel under 40% strain. (D) Force–strain curves of AgNWs/PVA gel under different humidification times. (E) Adhesion energy of AgNWs/PVA gel at various humidification times. (F) Resistance changes rate as a function of AgNWs/PVA gel tensile strain with different AgNWs concentrations. (G) Durability test of cyclic stretching/releasing for 500 cycles at 40% strain.

reinforcement provided by the AgNWs within the gel marix.[36] During the tensile testing, the high longitudinal modulus of AgNWs effectively dispersed stress, enhancing toughness. In addition, the interfacial bonding between AgNWs and the PVA matrix provides an additional energy dissipation pathway through physical embedding and van der Waals force, consistent with the "pull-out effect" observed in nano-reinforced composites, mitigating microcrack propagation and preventing damage.[37] However, once the concentration was above 1.5 g L^{-1}, it led to mechanical property degradation due to AgNWs aggregation, which disrupted the continuity of the gel matrix and weakened its reinforcement effects.[38]

As illustrated in Fig. 2B, the modulus and toughness of AgNWs/PVA gel are influenced by the variation of AgNWs concentration. At 1.5 g L^{-1} AgNWs concentration, the Young's modulus and toughness of the AgNWs/PVA gel reach 1.1 MPa and 7.1 MJ m^{-3}, respectively. AgNWs/PVA gel was cyclically stretched 1000 times at 40% strain (Fig. 2C), and this fatigue resistance highlights the long-term mechanical stability of AgNWs/PVA gel, thus verifying its reliability in long-term use.

Humidity from mist enhances skin adhesion due to the increased hydration of the PVA molecular chains, which facilitates stronger intermolecular interactions and better conformal contact with the skin surface. Fig. 2D demonstrates the force–distance curves of AgNWs/PVA gels under different humidification times. As humidification time increased, the area and peak values of the force curves first increased and then decreased, reaching a maximum value of 88.9 mN at 30 s humidification time. Swelling performance is demonstrated in Fig. S12 (ESI†), the result indicates that they are limited suitability for heavily water-saturated environments. Fig. 2E provides a quantitative analysis of the effect of humidification time on adhesion energy. When the humidification time was less than 30 s, the PVA network was not fully hydrated, limiting surface molecular contact and resulting in low adhesion force and energy. As humidification time increased, the hydration of PVA molecular chains strengthened, significantly enhancing adhesion force,[39] with maximum adhesion energy reaching 270.5 μJ cm^{-2} at 30 s humidification time. Beyond 30 s, excessive surface water layers weakened adhesion, reducing both the maximum adhesion force and adhesion energy.[40] The AgNWs/PVA gel maintains higher strength and stretchability under dry conditions, while its adhesion and conformability are enhanced when wet. Maintaining moderate moisture at the interface is vital for achieving an optimal balance of adhesion, softness, and stretchability in skin-mounted devices (Fig. S13, ESI†).

The incorporation of AgNWs established conductive pathways within the AgNWs/PVA gel, enhancing electrical conductivity and enabling excellent conductivity under a certain range of strain.[41] The strain–resistance behavior of the AgNWs/PVA gel was characterized by measuring the change in electrical resistance under applied mechanical strain, as shown in Fig. 2F. After 500 cycles at 40% strain, $\Delta R/R_0$ remained almost unchanged (Fig. 2G), indicating excellent durability. Although strain occasionally caused minor cracks in AgNWs connections, the toughness and resilience of the PVA matrix allowed the

network to reconstruct upon strain release, maintaining electrical conductivity.[42] Moreover, the nanoscale size and high flexibility of the AgNWs prevented significant fractures or plastic deformation over multiple cycles.[43] The inset plots of Fig. 2G (29th to 45th cycle, 269th to 285th cycle, and 439th to 455th cycle) reveal nearly identical $\Delta R/R_0$ fluctuations, highlighting the consistent response of AgNWs/PVA gel during stress relaxation. This property is particularly important for practical applications involving complex stress conditions, such as repetitive stretching and compressing.

2.3. High-fidelity EMG and ECG monitoring by ultrathin AgNWs/PVA gel

The ultrathin AgNWs/PVA gel exhibits exceptional air permeance, stretchability, adhesion, skin compliance, and thermal comfort, making it highly suitable for long-term, seamless attachment to human skin—a vital property for monitoring high-fidelity electrophysiological signals during daily activities. To demonstrate the effectiveness of the AgNWs/PVA gel for high-fidelity electrophysiological monitoring on the human skin, we utilized it for recording EMG and ECG.

Fig. 3A analyzes the skin contact impedance of the ultrathin AgNWs/PVA gel compared to a commercial gel after different wearing times. At 10 and 100 Hz, the AgNWs/PVA gel shows skin contact impedances of 50.4 kΩ and 28.6 kΩ, respectively—reducing impedance by 59 and 45% compared to a commercial gel electrode. These results confirm that the ultrathin AgNWs/PVA gel provides significantly lower skin contact impedance in the low-frequency range (10 Hz to 1 kHz). Additionally, the skin contact impedance of the AgNWs/PVA gel remains nearly constant after 8 h of wear, while the commercial gel exhibits a significant increase. This stability is attributed to the high skin affinity of the ultrathin gel, enabling the AgNWs/PVA gel to adapt to the microscopic undulations of human skin and maintain low contact interface resistance over extended periods.[42] In addition, the nearly identical impedance curves observed on days 1 and 14 confirm that the conductive network remains stable, indicating no chemical degradation occurs between AgNWs and PVA (Fig. S14, ESI†).

EMG signals are weak potential changes (0.1–5 mV) caused by the depolarization and repolarization of muscle fibers. They are used to analyze neuromuscular function, diagnose neurological and muscular disorders, and guide personalized rehabilitation.[44] Fig. 3B shows the electrode wiring and monitoring setup for electrophysiological monitoring by a signal recording system and a wireless module. Fig. 3C compares EMG signal acquisition from the ultrathin AgNWs/PVA gel and a commercial gel during the use of a grip strength device. The ultrathin AgNWs/PVA gel recorded higher amplitude and clearer EMG waveforms, corroborated by its superior SNR (Fig. 3D). Within a certain strength range, as muscles produce more force, their electrical activity increases, reflected in higher EMG signal amplitudes and SNR,[45] as shown in Fig. 3E and Fig. S15 (ESI†). Meanwhile, an increase in the SNR of the EMG signal was observed under sweating condition (Fig. S16, ESI†).

ECG is widely used to diagnose abnormalities such as coronary artery under perfusion, and electrolyte imbalances.[16]
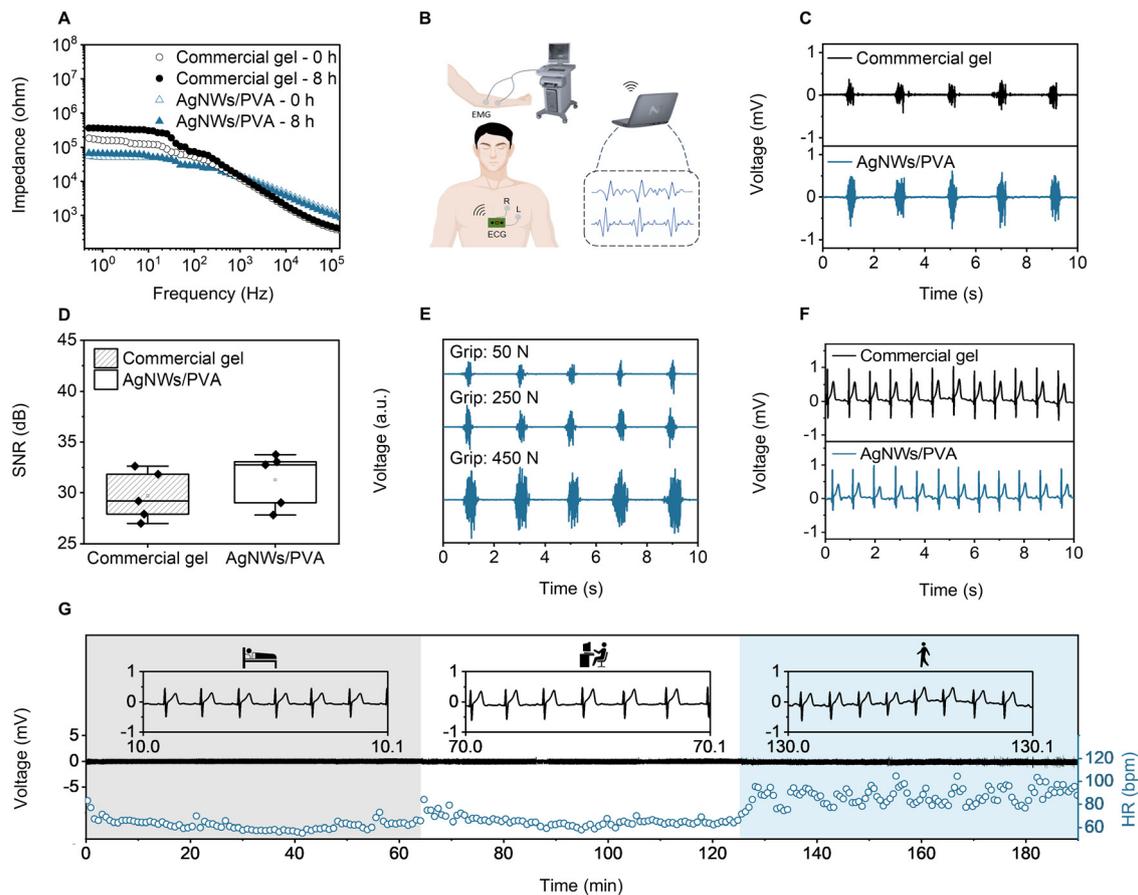
Fig. 3 High-fidelity EMG and ECG monitoring by ultrathin AgNWs/PVA gel. (A) Skin contact impedance of commercial gel and ultrathin AgNWs/PVA gel with different wearing duration. (B) Schematic illustration of the experimental setup for measuring EMG and ECG signals. (C) EMG monitoring by commercial gel (top) and ultrathin AgNWs/PVA gel (bottom) in the state of using the grip. (D) SNR of EMG signals measured by commercial gel and ultrathin AgNWs/PVA gel. (E) EMG signals produced by the muscles at different grip strengths were acquired by ultrathin AgNWs/PVA gel. (F) ECG monitoring by commercial gel (top) and ultrathin AgNWs/PVA gel (bottom) in a sedentary state. (G) AgNWs/PVA gel applied to 3 h ECG long-term monitoring under sleep (gray background), PC work (white background), and work out (blue background) states.

However, many cardiac events, especially those that occur occasionally under specific conditions like exercise or stress, are difficult to capture with traditional ECG measurements.[1,24] Fig. 3F compares the performance of a commercial gel with the ultrathin AgNWs/PVA gel in ECG monitoring. Both gels successfully capture high-fidelity ECG signals, including characteristic P, QRS, and T waves. The temporal characteristics and overall waveform patterns are consistent between the two gels. The SNR of the AgNWs/PVA gel averages 31.2 dB, comparable to the commercial gel (Fig. S17, ESI†), confirming that its performance in actual signal acquisition meets practical application standards.[46]

The performance of the ultrathin AgNWs/PVA gel was evaluated under various daily scenarios, including sleep, PC work, and work out. Fig. 3G presents 3 h continuous ECG monitoring using the ultrathin AgNWs/PVA gel during these activities. Throughout the monitoring process, the amplitude data of the signals remained consistent during sleep (gray background), PC work (white background), and work out (blue background). Notably, heart rate (HR) varied significantly with the scenarios: 60 beats per min (bpm) during sleep, 65 bpm during PC work,

and 75–105 bpm during work out. The lowest HR was around 60 bpm in the sleep scenario, the medium HR around 65 bpm during PC work, and the HR significantly higher in the work out scenario, fluctuating between 75 and 105 bpm. In low HR scenarios (sleep and PC work), the AgNWs/PVA gel maintained ideal skin contact with minimal mechanical interference, resulting in stable signal amplitude. In high HR scenarios (work out), artifacts introduced by motion may cause slight fluctuations in amplitude.[47] Despite this, the ECG waveforms remained clear across all scenarios, demonstrating the AgNWs/PVA gel's ability to provide reliable signal acquisition during both dynamic and static conditions in long-term monitoring.

2.4. High-fidelity and long-term EEG recording by ultrathin AgNWs/PVA gel

High-quality and noninvasive EEG recording is challenging due to weak signals in the microvolt range and interference from thick hair.[12] To address these issues, electrodes integrated with AgNWs/PVA gel were positioned at Fp1 (active electrode) and A1 (reference electrode) according to the 10–20 international EEG
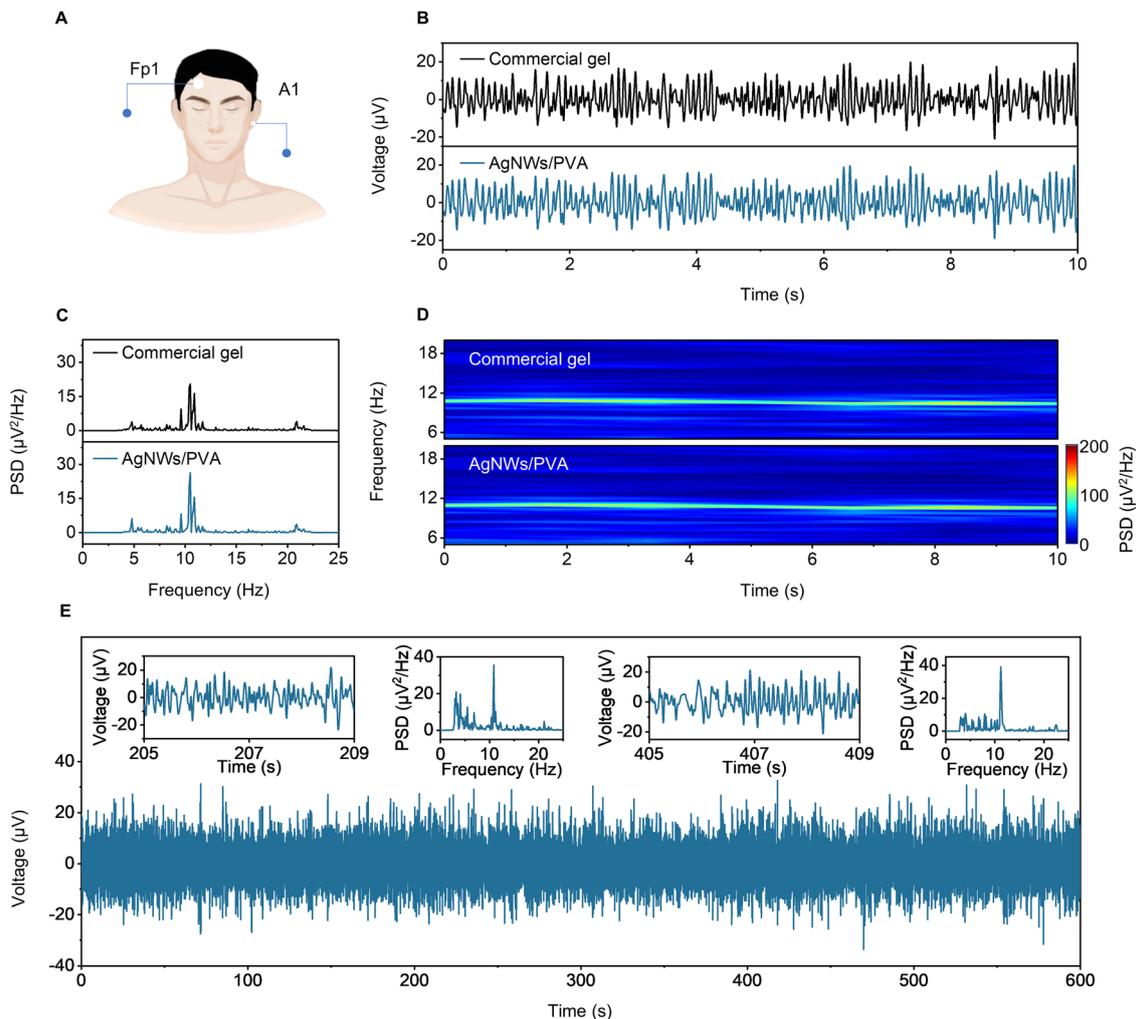
Fig. 4 High-fidelity and long-term EEG recording by ultrathin AgNWs/PVA gel. (A) Schematic illustration of the experimental setup for measuring EEG signals. (B) EEG alpha rhythms recorded by commercial gel (top) and ultrathin AgNWs/PVA gel (bottom) during eye closure. (C) PSD of EEG signals from commercial gel (top) and ultrathin AgNWs/PVA gel (bottom) in (B). (D) Spectrograms of EEG signals recorded by commercial gel (top) and ultrathin AgNWs/PVA gel (bottom) during eye closure. (E) Continuous 10 min EEG monitoring using ultrathin AgNWs/PVA gel during eye closure, with inset showing typical alpha rhythm and PSD during 205–207 and 405–407 s.

standard (Fig. 4A).[48] Fig. 4B compares the EEG signals recorded by the ultrathin AgNWs/PVA gel and a commercial gel during eye closure (10 s). The ultrathin AgNWs/PVA gel recorded EEG signal amplitudes of approximately ±20 μV, nearly identical to those of the commercial gel, with highly similar signal fluctuation characteristics.

Fig. 4C compares the performance of the AgNWs/PVA gel with that of the commercial gel in the frequency domain through power spectral density (PSD) analysis. Both gels exhibit clear and comparable PSD in the closed-eye alpha-wave frequency band (10 Hz).[49] Fig. 4D illustrates the spectrograms of EEG signals recorded by the AgNWs/PVA gel and the commercial gel during eye closure. Both gels demonstrated comparable performance in capturing core EEG signals (10 Hz alpha band), effectively recording high-intensity EEG signals.

Fig. 4E presents EEG signals continuously acquired by the ultrathin AgNWs/PVA gel over a 10 min period. Throughout the

signal collection process, the signal amplitude remained stable without significant drift, indicating the AgNWs/PVA gel's excellent stability for long-term monitoring—a crucial factor for reliable EEG detection.[50] The inset graphs show that during the localized time period of 205–207 and 405–407 s, the EEG signals recorded by the ultrathin AgNWs/PVA gel exhibited a typical alpha rhythm with clear waveforms and no distortion. This demonstrates that the AgNWs/PVA gel maintains stable performance in capturing key EEG frequency bands, underscoring its great potential for application in long-term brain activity monitoring.

3. Conclusion

In conclusion, we have successfully developed an ultrathin AgNWs/PVA gel that demonstrates exceptional tensile strength,

remarkable stretchability, robust adhesion, thermal comfort, and low skin contact impedance. These superior mechanical and electrical properties make the gel highly suitable for long-term, seamless attachment to human skin, a critical require-ment for reliable monitoring of electrophysiological signals during dynamic daily activities. Practical applications of the ultrathin AgNWs/PVA gel reveal that its SNR is on par with conventional commercial gels, while exhibiting enhanced stability during prolonged continuous ECG monitoring. The gel maintains consistent signal amplitude and clear waveform fidelity, accurately reflecting HR variations aligned with daily activities. Furthermore, comprehensive EMG and EEG monitor-ing validate the gel's capability to achieve high-fidelity signal acquisition across diverse intensities and scenarios. This adapt-ability underscores its suitability for complex environments and sustains electrophysiological monitoring. This work pre-sents a promising material solution that addresses the critical challenges in noninvasive, long-term health monitoring. The ultrathin AgNWs/PVA gel not only enhances the accuracy and reliability of EMG, ECG, and EEG recordings but also paves the way for advancements in personalized medicine and compre-hensive health surveillance. By combining nanomaterial rein-forcement with an ultrathin polymer matrix, this gel offers a new paradigm for epidermal electronics, ensuring both comfort and high performance. Future research is essential to reduce production cost while maintaining high-level performance.

4. Experiment section

4.1. Materials

Analytical pure phosphoric acid was supplied by Guangdong Guan-ghua Sci-Tech Co., Ltd. PVA (Mw: 89 000–98 000, 99 + % hydrolyzed) was obtained from Sigma-Aldrich. AgNWs with a concentration of 20 mg mL^{-1} and a diameter of 120 nm were sourced from Nanjing XFNANO Materials Tech Co., Ltd. Petri dishes with a diameter of 90 mm were acquired from Beijing Labgic Technology Co.

4.2. Fabrication of AgNWs/PVA gel

To fabricate the AgNWs/PVA gel, 1 g PVA was dissolved in 89 mL of deionized water by stirring in a water bath at 90 °C to obtain a homogeneous PVA solution. Subsequently, 0.9 mL of phosphoric acid was added to the PVA solution and stirred continuously for 12 h to ensure complete integration. Depend-ing on the desired concentration, between 2.5 mL and 10 mL of AgNWs suspension (20 mg mL^{-1}) was added to the solution at a stirring rate of 800 rpm, and the total volume was adjusted to 100 mL to obtain the AgNWs/PVA gel precast solution. A measured amount of the precast solution was then poured into a Petri dish. Finally, the mixture was placed in a 40 °C incubator for 8 h to facilitate gelation, resulting in the for-mation of the AgNWs/PVA gel.

4.3. Characterization of AgNWs/PVA gel

Optical micrographs of the samples were acquired using a mobile digital microscope (AM7515MT8A, Dino-Lite, Japan).

For more detailed imaging, a 3D measuring laser microscope was employed to obtain comprehensive optical micrographs of the samples. The samples were subjected to liquid nitrogen embrittlement to prepare them for SEM, which was conducted at 15 kV to observe the cross-sectional topographic features. Infrared thermal imaging was utilized to measure changes in skin temperature before and after exercise, with image data processed using FLIR Ignite Sync software. To assess the thickness of the samples, they were placed on a test platform, and a probe was slowly moved from the edge towards the center, with the height recorded by a probe profiler (DEKTAK-XT, Boyue Instruments, China). Hydrophilicity was evaluated through contact angle measurements performed on AgNWs/PVA gels fixed on glass slides. 0.6 µL water droplet was gently placed on the surface, and its interaction was captured by a contact angle meter (DSA25E, Kruss Scientific, Germany). The air permeance was evaluated by placing the sample in a low pressure membrane separator (HP-21, China) for measurement. A constant gas pressure was applied to the upstream chamber of the membrane while keeping the downstream chamber initially under vacuum or low pressure, and the pressure in the down-stream chamber was monitored over time. The air permeance was calculated from the pressure growth curve. The air per-meance (P) was calculated using the formula:

$$P = \frac{273}{76} \times \frac{V}{ATp} \times \frac{\mathrm{d}p}{\mathrm{d}t} \tag{1}$$

where P represents air permeance, V denotes the volume on the gas permeation side, A is the effective membrane area, T is the temperature, p refers to the pressure difference between the two sides of the specimen, and $\frac{\mathrm{d}p}{\mathrm{d}t}$ indicates the rate of pressure increase on the permeation side of the specimen.

4.4. Mechanical and tack separation test

The mechanical tensile properties of the samples were mea-sured using a tensile tester (Mark-10, ESM303, USA) equipped with a load cell. The sample was positioned on a polyimide frame (20 mm × 10 mm) and aligned vertically by attaching the tensile tester to the top and bottom of the frame. The left and right edges of both the sample and frame were carefully cut using a knife to ensure precise alignment. After adjusting the settings, the tensile test was performed as illustrated in Fig. S18 (ESI†).

For tack separation measurements, a 10 mm × 10 mm × 10 mm block of artificial skin was placed on the platform, and a 20 mm × 20 mm AgNWs/PVA gel sample was affixed to a polyimide frame. The sample was humidified by placing it 20 cm away from a humidifier (SC-3G40A, Midea, China) before transferring it to the test bench to ensure initial contact with the artificial skin (10 mm × 10 mm). The test bench was then lifted at a rate of 20 mm min^{-1} to gradually separate the sample from the artificial skin, with the adhesion force recorded by a

tensile tester as shown in Fig. S19 (ESI†). The adhesion energy (E) was calculated using the formula:

$$\text{Adhesion energy} = \int_0^x y\,\mathrm{d}L \qquad (2)$$

where y, x and L are separation force, separation stroke, and stroke, respectively.

4.5. Measurement of contact impedance and electromechanical properties

To measure the skin contact impedance, a pair of ultrathin 2 × 2 cm AgNWs/PVA gel was applied to the human forearm and measured using an electrochemical workstation (VersaSTAT 3, Princeton Applied Research, USA) with a frequency range of 10^5 to 10^{-1} Hz. The gel electrodes were tested for skin contact impedance at a center-to-center distance of 5 cm. Commercial gel electrodes of the same size were used for comparison.

To assess changes in electrical properties during stretching, samples were transferred from a polyimide frame to a motorized mobile stage (LTS150/M, Thorlabs, USA) and fixed in place. The ends of the samples were connected to the electrochemical workstation using wires. The motorized mobile stage was then used to stretch the samples to fracture, with resistance changes recorded continuously. For durability testing, the motorized mobile stage was programmed to cyclically stretch the samples for 500 cycles at 40% strain. Throughout these cycles, resistance data were continuously recorded by the electrochemical workstation.

4.6. Electrophysiological recording

For EMG monitoring, a pair of AgNWs/PVA gels with integrated flexible Ag/AgCl electrodes were affixed to the subject's radial flexor muscles as test electrodes, and additional integrated AgNWs/PVA gel electrodes were adhered to the dorsum of the hand as ground electrodes. All electrodes were connected to a signal recording system (MEB-2312C, Nihon Kohden, Japan) through a bandpass filter (10 Hz to 10 kHz), and commercial gel electrodes were used using the same procedure as a comparison. EMG signals were generated when the subject pressed and released with a fixed grip.

For wireless ECG signal recording, two AgNWs/PVA gels with integrated flexible Ag/AgCl electrodes were attached to the left chest of a male subject and connected to a commercial wireless module (GM3 Ltd., Japan), and the commercial gel electrodes were subjected to the same steps for comparison. The wireless module had recording, processing, and transmission circuits and used MATLAB software for data processing.

For EEG monitoring, a healthy male volunteer participated in the process of EEG recording. AgNWs/PVA gel with flexible Ag/AgCl electrodes were placed on a clean forehead Fp1 and commercial EEG paste was applied to the ear as a ground electrode according to the 10 to 20 International Electrode Placement System. Detailed sensor placement is shown in Fig. 4A. For comparison, the commercial gel was placed near the AgNWs/PVA gel at the same time. All electrodes were connected to a signal recording system with a band-pass filter (0.05 to 50 Hz)

for recording and processing. EEG signals were generated when subjects closed their eyes in a sedentary state.

Experiments on human subjects

All experiments of electrophysiological signals were thoroughly reviewed and approved by the internal ethical committee (approval number E20240902001), and informed consent was obtained from subjects participating in the experiment.

Author contributions

Y. W. conceived the concept. J. Y., J. Y. and Y. G. developed the materials and performed the characterization experiments. J. Y., Z. W., and Y. W. designed the EMG, ECG, and EEG experiments. J. Y., Q. S., and Z. W. performed the bio signal recording experiments. J. Y., W. Y., and Y. X. processed and analyzed the bio signal data. J. Y, P. Z., Z. W. and J. Z. participated in the discussion of the data and results, J. Y., Z. W. and X. H. performed the air permeance experiment. J. Y. analyzed the data and wrote the manuscript. Y. W. supervised the project. All authors participated in the revision of the manuscript.

Data availability

The data that support the findings of this study are available from the corresponding author upon reasonable request.

Conflicts of interest

The authors declare no conflict of interest.

Acknowledgements

References

1 Z. Lian, Y. Ding, Y. Chen, D. Yu and W. Wang, *Colloids Surf., A*, 2024, **703**, 135253.

2 H. Y. Duan, Y. L. Zhang, Y. T. Zhang, P. C. Zhu and Y. C. Mao, *Nanomaterials*, 2024, **14**, 1398.

3 S. Xia, M. Wang and G. H. Gao, *Nano Res.*, 2022, **15**, 9850–9865.

4 G. Luo, J. Xie, J. Liu, Q. Zhang, Y. Luo, M. Li, W. Zhou, K. Chen, Z. Li, P. Yang, L. Zhao, K. Siong Teh, X. Wang, L. Dong, R. Maeda and Z. Jiang, *Chem. Eng. J.*, 2023, **451**, 138549.

5 Y. Pan, X. Cui, D. Song, W. Hu, X. Lin and N. Liu, *ACS Appl. Nano Mater.*, 2024, **7**, 12064–12071.

6 Q. Liu, J. Zhou, Q. Zeng, D. Sun, B. Yu, L. Yang, Z. Zhang, J. Wu and Y. Zhang, *ACS Appl. Nano Mater.*, 2023, **7**, 18226–18236.

7 T. Fang, Y. Sun and D. Kong, *ACS Appl. Bio Mater.*, 2024, **7**, 7791–7798.

8 N. B. Alsaafeen, S. S. Bawazir, K. K. Jena, A. Seitak, B. Fatma, C. Pitsalidis, A. Khandoker and A.-M. Pappa, *ACS Appl. Mater. Interfaces*, 2024, **16**, 61435–61445.

9 S. Roubert Martinez, P. Le Floch, J. Liu and R. D. Howe, *Adv. Healthcare Mater.*, 2023, **12**, e2202661.

10 G. Wang, M. Liu, C. Zhang, S. Xia, G. Gao and Y. Shi, *Eur. Polym. J.*, 2024, **207**, 112843.

11 L. Pan, P. Cai, L. Mei, Y. Cheng, Y. Zeng, M. Wang, T. Wang, Y. Jiang, B. Ji, D. Li and X. Chen, *Adv. Mater.*, 2020, **32**, e2003723.

12 Z. Zhang, J. Yang, H. Wang, C. Wang, Y. Gu, Y. Xu, S. Lee, T. Yokota, H. Haick, T. Someya and Y. Wang, *Sci. Adv.*, 2024, **10**, eadj5389.

13 S. Cheng, Z. Lou, L. Zhang, H. Guo, Z. Wang, C. Guo, K. Fukuda, S. Ma, G. Wang, T. Someya, H. M. Cheng and X. Xu, *Adv. Mater.*, 2022, **35**, 2206793.

14 T. Li, Y. Ding, C. Teng, Y. Zheng, X. Wang and D. Zhou, *ACS Appl. Mater. Interfaces*, 2024, **16**, 60625–60632.

15 H.-L. Peng, T. Qian, T. Xian, C. Jiang, Y. Qin, Q. Li and S. Song, *Chem. Eng. J.*, 2024, **494**, 153138.

16 G. Li, Y. Gong, S. Fang, T. You, R. Shao, L. Yao, C. Liu, C. Wu, J. Niu and W.-Y. Lai, *Sci. China Mater.*, 2024, **67**, 1481–1490.

17 W. Zhou, S. Yao, H. Wang, Q. Du, Y. Ma and Y. Zhu, *ACS Nano*, 2020, **14**, 5798–5805.

18 S. Chen, K. Hou, T. Li, X. Wu, Z. Wang, L. Wei and W. L. Leong, *Adv. Mater. Technol.*, 2022, **8**, 2200611.

19 J. H. Shin, J. Y. Choi, K. June, H. Choi and T. I. Kim, *Adv. Mater.*, 2024, **36**, e2313157.

20 X. Yang, S. Wang, M. Liu, L. Li, Y. Zhao, Y. Wang, Y. Bai, Q. Lu, Z. Xiong, S. Feng and T. Zhang, *Small*, 2022, **18**, e2106477.

21 Y. Shi, T. Ding, Z. Yuan, R. Li, B. Wang and Z. Wu, *Nanoenergy Adv.*, 2022, **2**, 52–63.

22 S. Lee, S. Franklin, F. A. Hassani, T. Yokota, M. O. G. Nayeem, Y. Wang, R. Leib, G. Cheng, D. W. Franklin and T. Someya, *Science*, 2020, **370**, 966–970.

23 Y. Wang, S. Lee, T. Yokota, H. Wang, Z. Jiang, J. Wang, M. Koizumi and T. Someya, *Sci. Adv.*, 2020, **6**, eabb7043.

24 L. Li, X. Ye, Z. Ji, M. Zheng, S. Lin, M. Wang, J. Yang, P. Zhou, Z. Zhang, B. Wang, H. Wang and Y. Wang, *Small*, 2025, **21**, 2407996.

25 Y. Li, Y. Gu, S. Qian, S. Zheng, Y. Pang, L. Wang, B. Liu, S. Liu and Q. Zhao, *Nano Res.*, 2024, **17**, 5479–5490.

26 F. Wu, J. Gao, Y. Xiang and J. Yang, *Polymers*, 2023, **15**, 3782.

27 S. Azadi, S. Peng, S. A. Moshizi, M. Asadnia, J. Xu, I. Park, C. H. Wang and S. Wu, *Adv. Mater. Technol.*, 2020, **5**, 2000426.

28 L. Xu and D. Qiu, *Sci. China Mater.*, 2022, **65**, 547–552.

29 Z. Li, D. Wang, H. Bai, S. Zhang, P. Ma and W. Dong, *Macromol. Mater. Eng.*, 2020, **305**, 1900623.

30 Y. Wang, S. Lee, H. Wang, Z. Jiang, Y. Jimbo, C. Wang, B. Wang, J. J. Kim, M. Koizumi, T. Yokota and T. Someya, *Proc. Natl. Acad. Sci. U. S. A.*, 2021, **118**, e2111904118.

31 Y.-W. Kim, J.-M. Park, C. S. Park, H. Na, Y.-W. Kang, W. Lee and J.-Y. Sun, *ACS Appl. Mater. Interfaces*, 2024, **16**, 4013–4023.

32 Y. Zhao, X. Zhang, Y. Hao, Y. Zhao, P. Ding, W. Zhai, K. Dai, G. Zheng, C. Liu and C. Shen, *Adv. Compos. Hybrid Mater.*, 2024, **7**, 245.

33 S. Yao, J. Shen, Y. Guo, S. Zuo, F. Shi, J. Jiang and J. Chu, *J. Mater. Chem. B*, 2021, **9**, 8676–8685.

34 J. W. Jeong, W. H. Yeo, A. Akhtar, J. J. Norton, Y. J. Kwack, S. Li, S. Y. Jung, Y. Su, W. Lee, J. Xia, H. Cheng, Y. Huang, W. S. Choi, T. Bretl and J. A. Rogers, *Adv. Mater.*, 2013, **25**, 6839–6846.

35 Y. Zhao, L. Wang, Y. Zhang, S. Qiao, S. Liang, T. Zhou, X. Zhang, X. Guo, Z. Feng, F. Lan, Z. Chen, X. Yang and Z. Yang, *Nano Lett.*, 2019, **19**, 7588–7597.

36 I. K. Han, T. Chung, J. Han and Y. S. Kim, *Nano Convergence*, 2019, **6**, 18.

37 F. Liu, X. Han, X. Cui, Y. Cao, P. Bai, Z. Du, H. Wang and L. Jin, *Vacuum*, 2024, **222**, 113044.

38 Y. Zare, *Composites, Part A*, 2016, **84**, 158–164.

39 R. Song, X. Wang, M. Johnson, C. Milne, A. Lesniak-Podsiadlo, Y. Li, J. Lyu, Z. Li, C. Zhao, L. Yang, I. Lara-Sáez, A. Sigen and W. Wang, *Adv. Funct. Mater.*, 2024, **34**, 2313322.

40 P. Zhang, C. Zhao, T. Zhao, M. Liu and L. Jiang, *Adv. Sci.*, 2019, **6**, 1900996.

41 M. Han, W. Shen, X. Tong and J.-P. Corriou, *Sens. Actuators, B*, 2024, **406**, 135375.

42 Y. Chen, J. Li, J. Lu, M. Ding and Y. Chen, *Polym. Test.*, 2022, **108**, 107516.

43 X. Yang, L. Li, S. Wang, Q. Lu, Y. Bai, F. Sun, T. Li, Y. Li, Z. Wang, Y. Zhao, Y. Shi and T. Zhang, *Adv. Electron. Mater.*, 2020, **6**, 2000306.

44 B. Zhang, J. Li, J. Zhou, L. Chow, G. Zhao, Y. Huang, Z. Ma, Q. Zhang, Y. Yang, C. K. Yiu, J. Li, F. Chun, X. Huang, Y. Gao, P. Wu, S. Jia, H. Li, D. Li, Y. Liu, K. Yao, R. Shi, Z. Chen, B. L. Khoo, W. Yang, F. Wang, Z. Zheng, Z. Wang and X. Yu, *Nature*, 2024, **628**, 84–92.

45 Q. Zhang, M. Qu, X. Liu, Y. Cui, H. Hu, Q. Li, M. Jin, J. Xian, Z. Nie and C. Zhang, *Adv. Mater. Interfaces*, 2022, **10**, 2201735.

46 S. Mandal, A. Seth, V. Yadav, S. Kumari, M. Kumar and U. Ojha, *ACS Appl. Polym. Mater.*, 2019, **2**, 618–625.

47 L. Wu, A. Liu, C. Li and X. Chen, *Adv. Eng. Inform.*, 2024, **62**, 102831.

48 C. Wang, H. Wang, B. Wang, H. Miyata, Y. Wang, M. O. G. Nayeem, J. J. Kim, S. Lee, T. Yokota, H. Onodera and T. Someya, *Sci. Adv.*, 2022, **8**, eabo1396.

49 V. Dimakopoulos, M. C. Neidert and J. Sarnthein, *Clin. Neurophysiol.*, 2023, **153**, 133–140.

50 Q. Han, C. Zhang, T. Guo, Y. Tian, W. Song, J. Lei, Q. Li, A. Wang, M. Zhang, S. Bai and X. Yan, *Adv. Mater.*, 2023, **35**, 2209606.